# Vector field path following and obstacle avoidance singularity mitigation via look-ahead flight envelope

First A. Author* and Second B. Author Jr.†
*Business or Academic Affiliation 1, City, State, Zip Code*

**Unmanned Aerial Vehicles conventionally navigate by following a series of pre-planned waypoints that may have to be re-planned when flying in a dynamic environment or encountering previously unknown obstacles. Waypoints are generally planned off-line and relayed to the UAV, taking up time and autopilot communication resources. Attractive path following and repulsive obstacle avoidance vector fields have been summed together to produce UAV guidance that follows pre-planned paths and avoids obstacles without the need to re-plan. Summing attractive and repulsive vector fields may produce small regions of null guidance, called singularities, which could potentially lead to trap situations. An investigation into singularity mitigation by vector field weight parameterization is presented.**

## I. Nomenclature

| | | |
|---|---|---|
| $UAV$ | = | Unmanned Aerial Vehicle |
| $VF$ | = | Vector Field |
| $VFF$ | = | Virtual Force Field |
| $LVF$ | = | Lyapunov Vector Field |
| $GVF$ | = | Goncalves Vector Field |
| $\overrightarrow{X}$ | = | UAV position |
| $\overrightarrow{U}$ | = | UAV velocity |
| $\theta$ | = | UAV heading |
| $\dot{\theta}$ | = | UAV heading rate |
| $u$ | = | UAV speed |
| $dt$ | = | discrete time step |
| $\overrightarrow{V}_{conv}$ | = | Convergence Vector |
| $\overrightarrow{V}_{circ}$ | = | Circulation Vector |
| $G$ | = | Convergence Weight |
| $H$ | = | Circulation Weight |
| $V$ | = | Potential Function |
| $r_O$ | = | Obstacle Radius |
| $R$ | = | Decay Radius |
| $\gamma$ | = | Path Deviation Cost |
| $\alpha_i$ | = | Surface Function |
| $x$ | = | UAV horizontal position |
| $y$ | = | UAV vertical position |
| $x_c$ | = | Circular obstacle horizontal position |
| $y_c$ | = | Circular obstacle vertical position |
| $d$ | = | Range to obstacle |
| $P$ | = | Obstacle Decay Weight |

*Insert Job Title, Department Name, Address/Mail Stop, and AIAA Member Grade (if any) for first author.
†Insert Job Title, Department Name, Address/Mail Stop, and AIAA Member Grade (if any) for second author.

## II. Introduction

Unmanned aerial vehicles (UAV)s are pilotless aircraft used by military, police, and civilian communities for tasks such as damage assessment [1], surveying [2], and target tracking [3–6]. Many UAV tasks depend on the vehicle's ability to autonomously follow a path while potentially avoiding obstacles and no-fly zones. Flight paths are typically followed by implementing guidance systems such as waypoint, carrot chasing, proportional-integral-derivative (PID), non-linear guidance laws, or linear quadratic regulator (LQR). Conventional path following guidance systems are typically not capable of avoiding obstacles without partially or completely re-planning the path. Paths are typically generated on a remote ground station and relayed to the UAV's autopilot. Updating a mission may be impossible under certain conditions, such as flying beyond line-of-sight. Avoiding obstacles without path re-planning has been achieved with potential field [7, 8] and vector field [3, 9–12] guidance methods.

Potential field employs the use of artificial attractive and repulsive forces that direct a UAV towards a goal while locally pushing away from nearby obstacles. Potential field may cause excess deviation from the desired path and provides guidance for converging to a singular point which is not ideal for fixed wing UAVs. A different VF technique, Gradient vector field (GVF), provides a continuous heading guidance that directs a UAV to converge and follow an arbitrary path that lies at the intersection of surfaces. The GVF method was modified in the standoff tracking scenario in [wwc] to include obstacle avoidance by summing an attractive GVF with repulsive obstacle GVFs. The repulsive GVFs pushed the UAV away from keep-out zones while allowing the UAV to return to the desired path.

The standoff tracking scenario in [wwc] did not address the possibility of attractive and repulsive vector fields canceling, leading to guidance singularities. Additionally, no optimized method for determining the radius of the decay field was specified to minimize deviation from the planned path. A method for locating singularities in a summed vector field is presented, followed by an improved GVF for circular obstacle avoidance method. The improved GVF will be compared in simulation to waypoint and potential field and planned path deviation compared for a worst-case head on collision scenario.

## III. Literature

UAVs are often used for tasks such as surveillance and data collection which require the UAV to fly closely to a pre-planned path. The pre-planned paths may represent a route where valuable data needs to be collected or an urban corridor that needs to be navigated carefully to avoid collision with known obstacles or no-fly zones. Remaining close to the planned path is essential for safe and efficient operation of the vehicle. Obstacles or no-fly zones that are discovered after a path has been planned would traditionally require that a new obstacle free and flyable path be recalculated and relayed to the UAV. These paths are commonly represented as a series of finite waypoints in commercial UAV autopilots such as the Piccolo [13], Kestral [14], and Pixhawk [15]. The on-board autopilot aligns the vehicle with the current active waypoint and switches to the subsequent waypoint once the UAV has reached a defined distance from the waypoint's center, referred to as the waypoint radius.

Avoiding obstacles with waypoint guidance may be accomplished by creating diversion waypoints off the planned path and outside of the obstacle. A single diversion waypoint may be enough to direct the UAV away from the obstacle, however may result in excess deviation from the planned path. Increasing the number of deviation waypoint may allow for the UAV to travel more of the planned path prior to deviating to avoid the obstacle. When it is not possible to plan a new obstacle free path, such as when the UAV is not able to communicate with the ground station, it may be beneficial to use a guidance system that can avoid obstacles without the path re-planning. Methods for obstacle avoidance guidance can be found in potential field and vector field guidance.

Potential field is based on the principle of artificial attractive and repulsive forces acting on a point mass to guide a system to a desired goal while avoiding static and dynamic obstacles [16]. Goals are represented as an attractive force that pull a point mass in the direction of minimal energy while obstacles are represented as repulsive forces that act locally to push the point mass away. Potential field is also capable of acting as a path and trajectory planning algorithm [17], possibly eliminating the off-board path planner. An example of potential field can be found in [7, 8, 18] which allowed for real time goal seeking with obstacle avoidance on a mobile ground robot equipped with ultrasonic sensors. The robot was attracted towards a goal with constant magnitude force. In the immediate area of the robot, an active window exists which records integer certainty values inside discrete cells. Cells containing an obstacle provide a

repulsive force opposite in direction to the line-of-sight from vehicle to cell location. The total repulsive force exerted on the robot is determined by summing the active cells. Summing together attractive and repulsive forces produce a vector that can be used for heading guidance.

Major drawbacks to potential field were identified in [18] consisting of local minimum and oscillations in corridors. The local minimum problem occurs when closely spaced obstacle's potential combine to produce a well on the descent gradient where a pre-mature stable point is reached. Proposed solutions to local minimum include object clustering and virtual waypoint method [19], virtual escaping route [20], and use of navigation functions [21]. Oscillations in potential field were addressed in [22] and [23]. In addition to local minimum and oscillations, potential field may not be ideal for providing guidance to return to a sensor path after avoiding an obstacle. Once the obstacle has been avoided, the attractive goal will direct the UAV in a straight path which may not lie along the sensor line. Guidance that follows an explicit path, deviates when necessary to avoid obstacles, and return back to the explicit path quickly can be accomplished with path following vector fields.

Vector fields produce continuous heading guidance that asymptotically converges and circulates a path. A comparison between vector field and waypoint guidance techniques was presented in [24] where each method was evaluated based on its complexity, robustness, and accuracy. The vector field model produced guidance that was both robust to external wind disturbances while maintaining a low cross track error. The two most prominent methods for generating vector fields in literature consist of the Lyapunov Vector Field (LVF) [3, 9, 25–28] and Gradient Vector Field (GVF) [10–12, 29] method. LVFs for converging and following straight and circular paths were described in [25]. Straight and circular path vector fields can be selectively activated throughout flight to form more complex paths, shown in [25–27, 30]. LVF for curved path following was presented in [9] which may allow for more complex paths and eliminates the need to switch between vector fields.

The Gradient Vector Field (GVF) method produces a similar field to LVF, however has several advantages over LVFs. GVF produces an $n$-dimensional vector field that converges and circulates to both static and time varying paths, which may be useful for tracking dynamic paths or avoiding dynamic obstacles. Additionally, convergence, circulation, and time-varying terms that make up the GVF are decoupled from each other allowing for easy weighting of the total field. GVFs converge and circulate at the intersection, or level set, of $n-1$ dimensional implicit surfaces ($\alpha_i : \mathbb{R}^n \rightarrow \mathbb{R} | i = 1, ..., n-1$). The integral lines of the field are guaranteed to converge and circulate the level set when two conditions are met: 1) the implicit surface functions are positive definite and 2) have bounded derivatives.
The total vector field for a time invariant path $\overrightarrow{V}$ is calculated by:

$$\overrightarrow{V} = G\nabla V + H \wedge_{i=1}^{n-1} \nabla\alpha_i \tag{1}$$

or in component form:

$$\overrightarrow{V} = G\overrightarrow{V}_{conv} + H\overrightarrow{V}_{circ} \tag{2}$$

where $\overrightarrow{V}_{conv}$ produces vectors that converge to the path and $\overrightarrow{V}_{circ}$ produces vectors that circulate the path. The multiplicative factors $G$ and $H$ are scalar weights to influence the strength of each field component.
Convergence is calculated by:

$$\overrightarrow{V}_{conv} = \nabla V \tag{3}$$

where the potential function $V$ is:

$$V = -\sqrt{{\alpha_1}^2 + {\alpha_2}^2} \tag{4}$$

$$\nabla V = \begin{bmatrix} \frac{dV}{dx} \\ \frac{dV}{dy} \\ \frac{dV}{dz} \end{bmatrix} \tag{5}$$

Circulation is calculated by taking the wedge product of the gradients of the surface functions:

$$\overrightarrow{V}_{circ} = \wedge_{i=1}^{n-1} \nabla\alpha_i \tag{6}$$

In the case of ($n = 3$) the wedge product simplifies as the cross product:

$$\overrightarrow{V}_{circ} = \nabla\alpha_1 \times \nabla\alpha_2 \tag{7}$$

The performance of Lyapunov [3] and gradient vector field [10–12] were compared for their cross track error with respect to the loiter circle in [WWC] and it was shown that gradient vector field had superior path tracking performance due to compensation for a time-varying vector field. The gradient vector field technique also has the benefit of decoupled weighting parameters for convergence, circulation, and time-varying terms, allowing customized field behavior without resolving the Lyapunov functions.

A circular time-varying attractive vector $\overrightarrow{V}_{path}$ field was attached to a moving ground target. Static circular repulsive vector fields $\overrightarrow{V}_o$ centered at the obstacles and weighted by hyperbolic tangent decay functions $P$, based on range from UAV to obstacle center, were summed with the attractive circular field to produce a target loitering, and obstacle avoidance guidance, shown in Equation 8.

$$\overrightarrow{V}_g = \overrightarrow{V}_{path} + P\overrightarrow{V}_o \tag{8}$$

Summing GVFs may result in guidance singularities where the two fields cancel. The presence of singularities were mentioned briefly in [25] and observed in [31]. For fixed wing UAVs the lack of guidance may prevent the UAV from avoiding an obstacle, while multi-rotor UAVs may end up in a trap situation. Methods for detecting singularities in a summed GVF guidance and selecting repulsive field decay radius and circulation weights for an optimized circular obstacle avoidance is the contribution of this research. The improved GVF guidance is shown to have an improved performance over waypoint guidance and potential field without the need re-plan mission paths.

### A. Dubins Model

The dynamics of UAVs can be represented by modeling the UAV as a Dubin's vehicle [3, 9, 25–27]. It is assumed that the autopilots control system is capable of maintaining stability, speed $u$, and can turn the vehicle at a fixed turn rate $\dot{\theta}$. The position of the UAV $\overrightarrow{X}$ at time $t$ is calculated from the integral of the velocity vector $\overrightarrow{U}$, Equation 10. Heading is an input from a guidance system, such as waypoint, potential field, or vector field.

$$\overrightarrow{U}(t) = u \begin{bmatrix} cos(\theta(t)) \\ sin(\theta(t)) \end{bmatrix} \tag{9}$$

$$\overrightarrow{X}(t) = \overrightarrow{U}dt + \overrightarrow{X}(t-1) \tag{10}$$

$$\dot{\theta} \leq 20deg/s \tag{11}$$

## IV. Methods

Optimizing GVF obstacle decay radius and circulation weight for minimizing deviation from a planned path and detecting GVF singularities is the objective of this research. Guidance for converging and following a straight path using GVF is presented along with the effects of modifying path circulation weights. A circular obstacle is represented as a repulsive GVF and summed with path following guidance. The contribution of this work is to present singularity detection in the summed field with strictly repulsive GVF obstacle and compared to an obstacle field with circulation. Additionally, A method for selecting GVF decay radius and circulation for an optimized obstacle avoidance is presented. Lastly, simulations comparing the improved GVF guidance to waypoint and potential field is shown.

### A. Optimal Avoidance Route for Straight Path

A geometrically optimal route around a circular obstacle can be used to compare the performance of avoidance algorithms. The path for avoiding a circular obstacle while maximizing the sensor path coverage can be accomplished with three circular arc turns. The circular obstacle is defined to have a radius $R$ and a lateral distance $Y_0$ from the sensor path in frame $I$. The first and third arc utilize the UAVs minimum turning radius, $\theta_r$, calculated in Equation 12. The start of the first minimum radius turn begins when the UAV's horizontal position $x$ reaches $\tilde{x}$ from the path frame origin. At a horizontal position $-\hat{x}$ the UAV turns with a radius of the obstacle $R$ and exits when the UAVs horizontal position reaches $\hat{x}$.

$$\theta_r = \frac{u}{\dot{\theta}} \tag{12}$$

The horizontal points $\tilde{x}$ and $\hat{x}$ are shown in Equations 13 and 14 respectively.

$$\widetilde{x} = -\sqrt{(\theta_r + R)^2 - (\theta_r - Y_o)^2} \tag{13}$$

$$\hat{x} = \frac{R\sqrt{(r + R)^2 - (\theta_r - Y_o)^2}}{R + \theta_r} \tag{14}$$

The avoidance path for navigating around a circular obstacle with maximum coverage of a sensor line is defined in Equation 15 and shown in Figure 1.

$$y(x) = \begin{cases} \widetilde{y} - \sqrt{\theta_r^2 - (x - \widetilde{x})^2} & x < -\hat{x} \\ Y_o + \sqrt{R^2 - x^2} & -\hat{x} \leq x \geq \hat{x} \\ \widetilde{y} - \sqrt{\theta_r^2 - (x + \widetilde{x})^2} & x > -\hat{x} \end{cases} \tag{15}$$

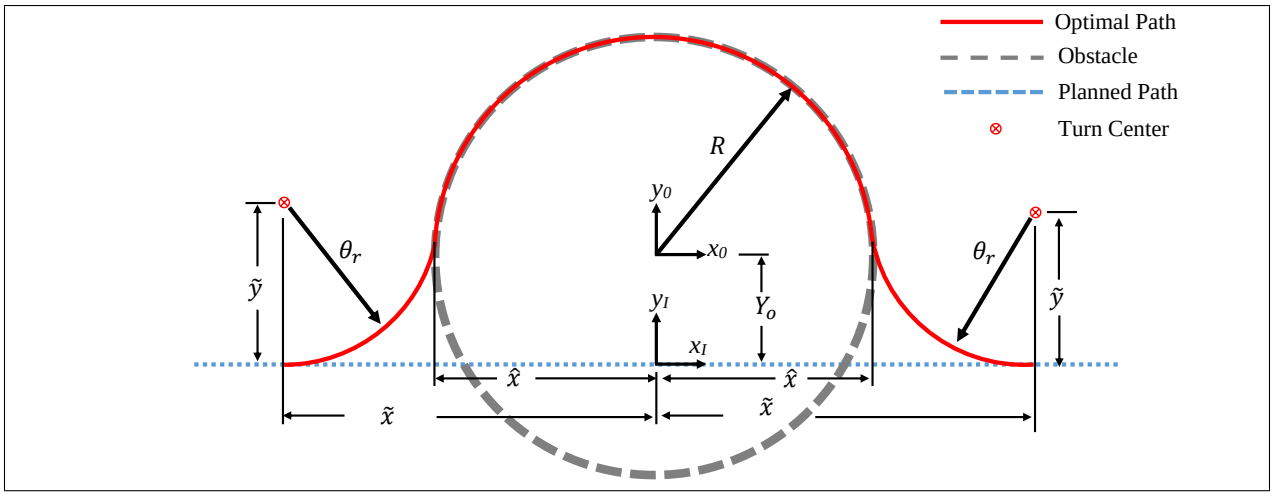


**Fig. 1 Optimal Kinematic Path Around Circular Obstacle**

The avoidance path represents the optimal path around a circular obstacle and would be used to generate waypoints for waypoint guidance.

### B. Path Following with GVF

Straight path following guidance of a time invariant line for a planar UAV at position $(x, y)$ is achieved by summing together convergence $\overrightarrow{V}_{conv}$ and circulation $\overrightarrow{V}_{circ}$ terms shown in Equation 2. The GVF converges and circulates at the intersection of two implicit surfaces, and for a straight path those surfaces are represented by planes. The implicit surface function $\alpha_1$ is at angle $\delta$ and plane $\alpha_2$ is at constant height of $Z = 1$ shown in Equations 16 and 17 respectively. The surfaces are depicted in Figure 2.

$$\alpha_1 = cos(\delta)x + sin(\delta)y \tag{16}$$

$$\alpha_2 = z \tag{17}$$

The gradient potential, $\nabla V$ is shown in Equation 18.

$$\nabla V = -\frac{1}{2(\sqrt{\cos^2(\delta)x^2 + 2\cos(\delta)\sin(\delta)xy + \sin^2(\delta)y^2})} \begin{bmatrix} 2x\cos^2(\delta) + 2\cos(\delta)\sin(\delta)y \\ 2y\sin^2(\delta) + 2\cos(\delta)\sin(\delta)x \\ 2 \end{bmatrix} \tag{18}$$

Circulation is calculated by the cross product of the surface function gradients, which evaluates to that shown in Equation 19.

$$\overrightarrow{V}_{circ} = \begin{bmatrix} sin(\theta) \\ -cos(\theta) \\ 0 \end{bmatrix} \tag{19}$$

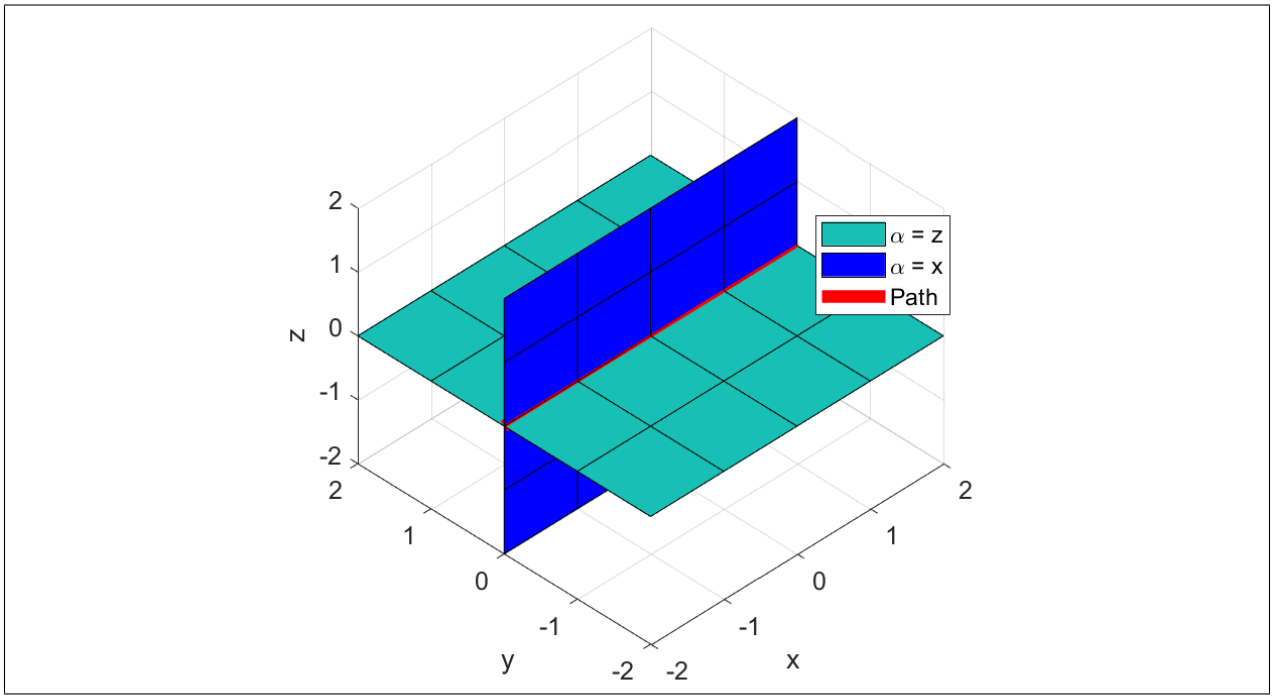


**Fig. 2 Plane intersection**

Guidance for a path at angle $\delta = 0$ and equal parts circulation and convergence weights $G = H = 1$ is shown in Figure 3. How quickly the path following field transitions from convergence to circulation depends on the field weights. Equal parts convergence and circulation are shown in Figure 3a ($G = H = 1$) and a larger circulation value in Figure 3b ($G = 1, H = 5$).

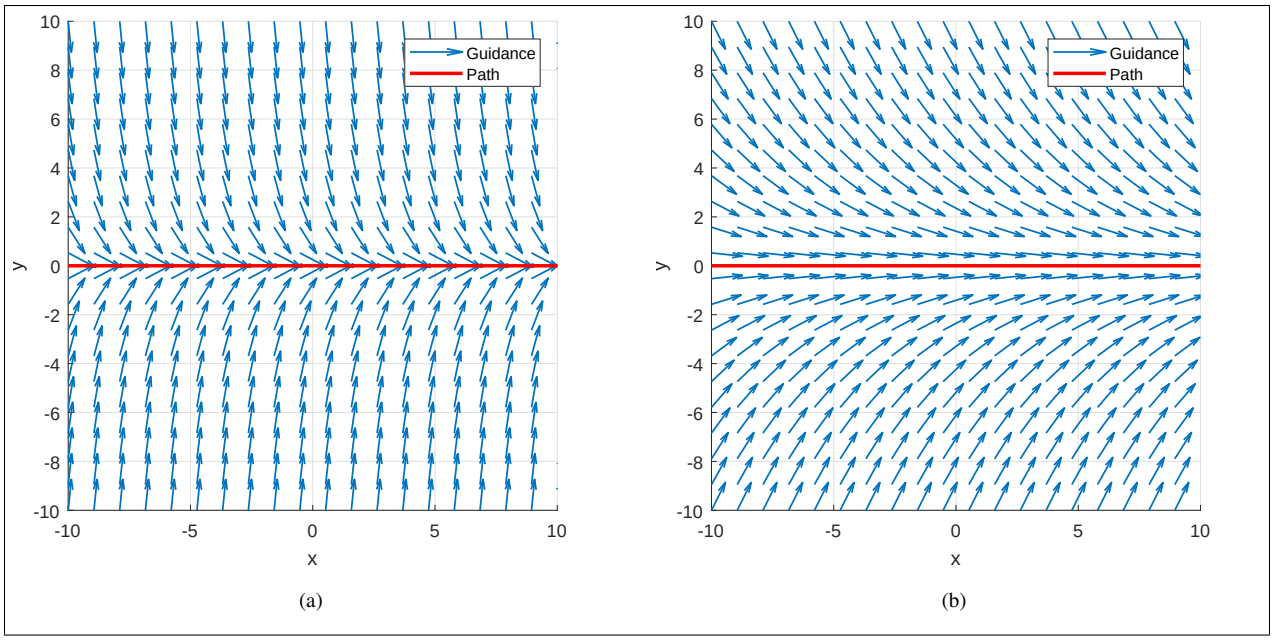


**Fig. 3 GVF converging and a) H=1 b) H=5**

### C. Avoidance

Previous works [wwc] avoided obstacles with a circular GVF modified with a tangent hyperbolic decay function. The circular avoidance vector field centered at $(x_c, y_c)$ and with radius $r$ is constructed by intersecting a cylinder, Equation 20, and a plane Equation 17.

$$\alpha_1 = (x - x_c)^2 + (y - y_c)^2 - r^2 \tag{20}$$

Convergence is calculated by the gradient of the potential function 18, which evaluates to

$$\nabla V = A\overrightarrow{B} \tag{21}$$

where

$$A = \frac{-1}{\sqrt{\bar{x}^4 + \bar{y}^4 + 2\bar{x}^2\bar{y}^2 - 2r^2\bar{x}^2 - 2r^2\bar{y}^2 + r^2 + z^2}} \tag{22}$$

$$\overrightarrow{B} = \begin{bmatrix} 2\bar{x}^3 + 2\bar{x}\bar{y}^2 - 2r^2\bar{x} \\ 2\bar{y}^3 + 2\bar{x}^2\bar{y} - 2r^2\bar{y} \\ z \end{bmatrix} \tag{23}$$

and

$$\bar{x} = x - x_c \tag{24}$$

$$\bar{y} = y - y_c \tag{25}$$

Circulation is calculated from the cross product of each implicit surface function's gradient, which equates to

$$\overrightarrow{V}_{circ} = \begin{bmatrix} 2(y - y_c) \\ -2(x - x_c) \\ 0 \end{bmatrix} \tag{26}$$

Strictly repulsion guidance is produced by assigning a negative weight to the convergence term $G = -1$, no circulation $H = 0$, and a small path radius $r$ to prevent trap situations. Limiting the distance at which the field has influence is achieved with a decay function shown in Equation 27 where $d$ is the range to the center of the obstacle and $R$ is the radius where the field has near zero strength.

$$P = -\tanh\left(\frac{2\pi d}{R} - \pi\right) + 1 \tag{27}$$

$$d = \sqrt{\bar{x}^2 + \bar{y}^2} \tag{28}$$

A strictly repulsive field $\overrightarrow{V}_{obst}$ with $G = -1$, $H = 0$, $r = 0.01$, and $R = 35$ is shown in Figure 4a. Adding equal magnitude circulation and decay $G = -1$, $H = 1$ is shown in Figure 4b to demonstrate the effects of circulation on an avoidance field.

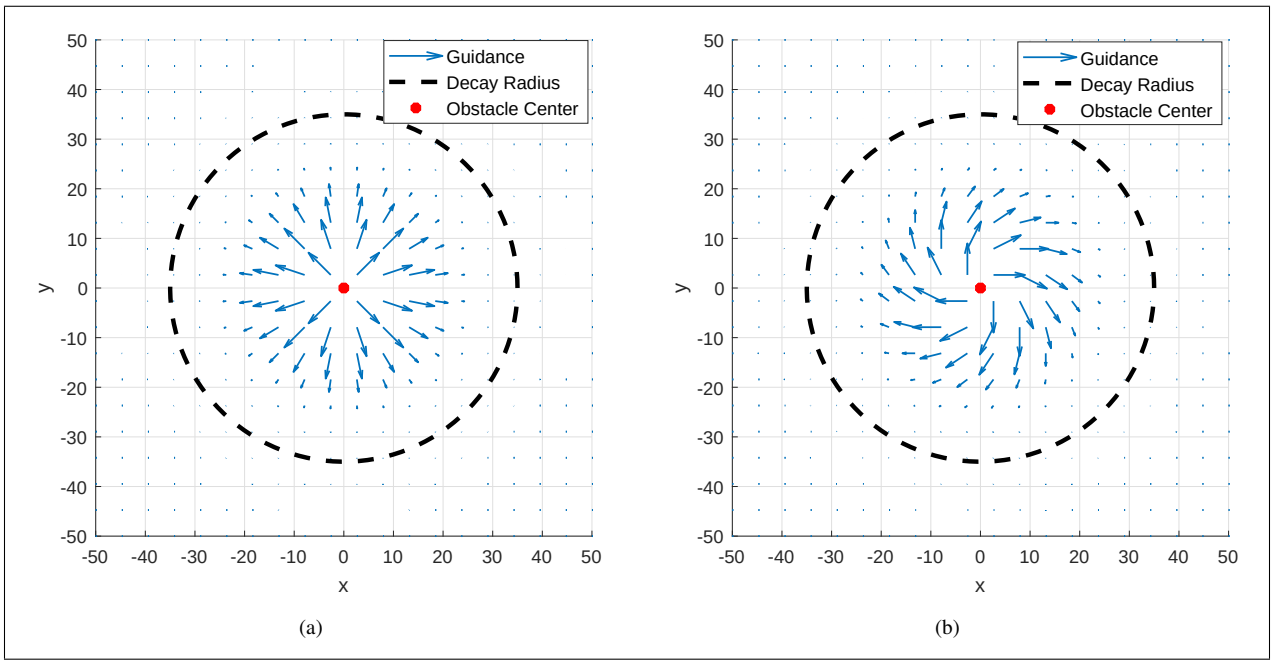


**Fig. 4 Repulsive GVF a) no circulation and b) with circulation**

Path following guidance and repulsive obstacle avoidance is achieved by summing the two fields together, shown in Equation 8.

### D. Singularity Detection

Summing vector field guidance may result in singularities, regions regions where vectors directly and equally oppose each other resulting in a null guidance. Singularities may be problematic if the UAV passes directly through one, which may result in trap situations or failure to avoid an obstacle. Singularities may exist where the magnitude of the vector $\overrightarrow{V}_g$ has a magnitude equal to zero, shown in Equation 29. Analytical solutions to singularity condition may be difficult to obtain when the path is non-linear and multiple solutions may also exist. A numerical search with initial conditions placed at the radius of equal strength, $R/2$, can be used to determine the location of singularities in the summed GVF guidance.

$$||\overrightarrow{V}_g|| = 0 \tag{29}$$

### E. Static Modified Weights

Determining the decay radius $R$ and circulation weight $H$ for a repulsive vector field depends on the UAVs speed $u$ and turnrate $\dot{\theta}$. An obstacle located at a lateral distance $Y_0$ from the pre-planned sensor path has a radius $r_O$ equal to a

scalar multiple of the UAVs turn radius, shown in Equation 30. The multiple $m$ is bounded on the interval $[1, \infty)$.

$$r_O = m\theta_r \tag{30}$$

The repulsive field decay radius $R$, expressed in $k$ multiples of the obstacles radius is shown in Equation 31 and also bounded on the interval $[1, \infty)$.

$$R = kr_O \tag{31}$$

The decay multiple $k$ and circulation $H$ are then determined by minimizing the cost function 32, where $y$ is the lateral deviation from the path in the $I$ frame and the function $j$ penalizes the UAV for entering the obstacle radius. The sign of $H$ can be determined from the LOS angle between the UAV and the obstacle such that the UAV travels around the obstacle in the correct, least distance, direction.

$$\underset{H,k}{\text{minimize}} \quad \frac{1}{R}\int_0^{t_f} y dt + j(x, y) \tag{32}$$

$$j(x, y) = \begin{cases} 100dt & \sqrt{(x - xc)^2 + (y - yc)^2} \leq r_O \\ 0 & \sqrt{(x - xc)^2 + (y - yc)^2} > r_O \end{cases} \tag{33}$$

A comparison of a UAVs route using a strictly repulsive vector field versus a vector field with circulation is shown in Figure 5. A UAV with a speed of $u = 20m/s$ and turning rate of $\dot{\theta} = 20deg/s$ following a straight vector field path is shown avoiding an obstacle of radius $m = 1$. The optimized GVF shows a decrease in the path deviation function compared to the non-optimized GVF of 72%.

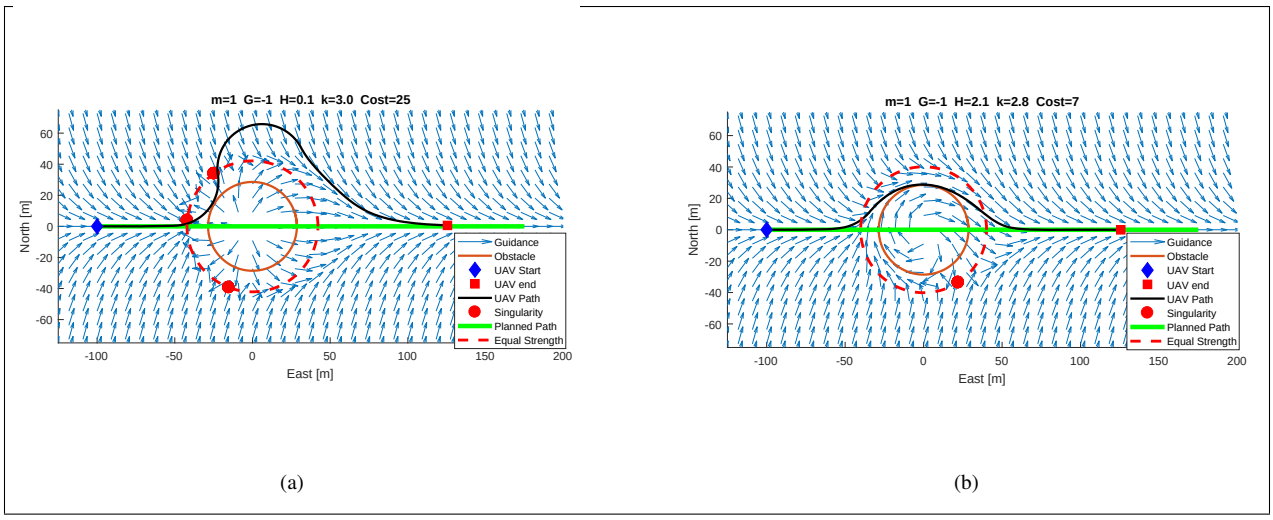


**Fig. 5 Repulsive and Circulating VF Guidance UAV Route**

The definition of obstacle and decay field radius in terms of vehicle turn radius $\theta_r$ allows for a single decay factor $k$ and circulation $H$ to be applicable for multiple velocities. This generalizes the avoidance field parameter selection problem and allows for a two dimensional lookup table to be generated for a number of obstacle radius factors $m$ and obstacle lateral positions $Y_0$ for real time obstacle avoidance.

## V. Simulations

A worst case avoidance scenario will be used to compare the optimized GVF with waypoint, VFF, and the optimal path with respect to the path deviation cost function. A circular obstacle centered on the path, $y_o = 0$, requires a deviation from the path of at least 50% of the obstacles radius. A fixed wing UAV at an initial position $(-400, 0)$ and heading $\theta = 0°$ follows the straight path connecting the points $(-400, 0)$ and $(400, 0)$ respectively. Traveling at a constant

speed $u = 25m/s$ and with a fixed turn rate of $\dot{\theta} = 20deg/s$ the UAV must avoid an obstacle with radius $2\theta_r$ located at the origin $(0, 0)$. The VFF guidance from [7] is used with an obstacle window radius of $\theta_r + r_o$, a cell repulsion $Fr = -3$, attraction force $F_t = 0.8$, range exponent $n = 2$, and a goal located at $(700, 0)$. For LOS waypoint guidance, 7 waypoints with a small waypoint radius of $10m$ was chosen. Each diversion waypoint added drives the guidance closer to optimal, however has diminishing returns past $6 - 7$ waypoints. GVF guidance with a circular repulsive field was assigned a convergence weight $G = -1$ and circulation and decay radius coefficient $k$ were determined by evaluating the cost function in Equation 32 with initial conditions $k_i = 2$ and $H = 2$. The GVF solution was bounded such that $2 \leq k \leq 4$ and $1 \leq H \leq 6$. Minimizing the cost function resulted in a decay radius coefficient $k = 2.78$ and a circulation value $H = 1.88$. The Dubin's paths for the three guidance methods discussed is shown in Figure 6.

VFF results in a UAV route that has excess deviation from the planned path with excessive turns. Waypoint guidance returns to the path more quickly than VFF, however deviates from the planned path farther then necessary. GVF leaves the path before waypoint guidance and tracks the outside of the obstacle closely and then quickly converges back to the pre-planned path. The cost of each method, defined in Equation 32, is displayed in the bar plot shown in Figure 7.

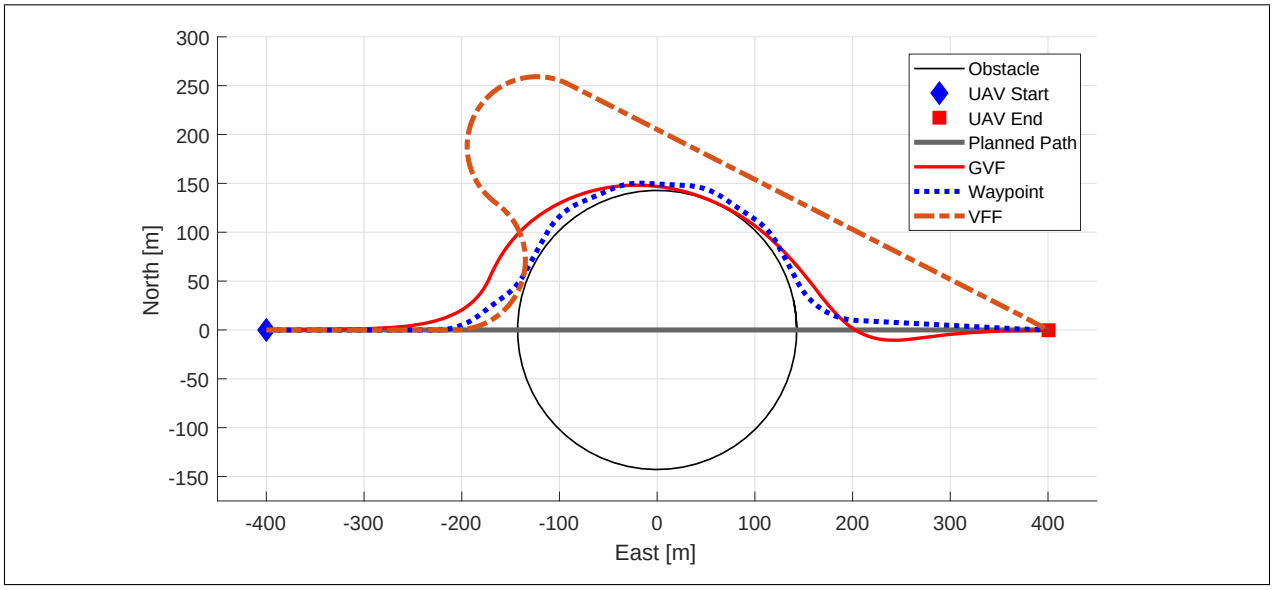


**Fig. 6 Path of UAV guided by guidance methods**

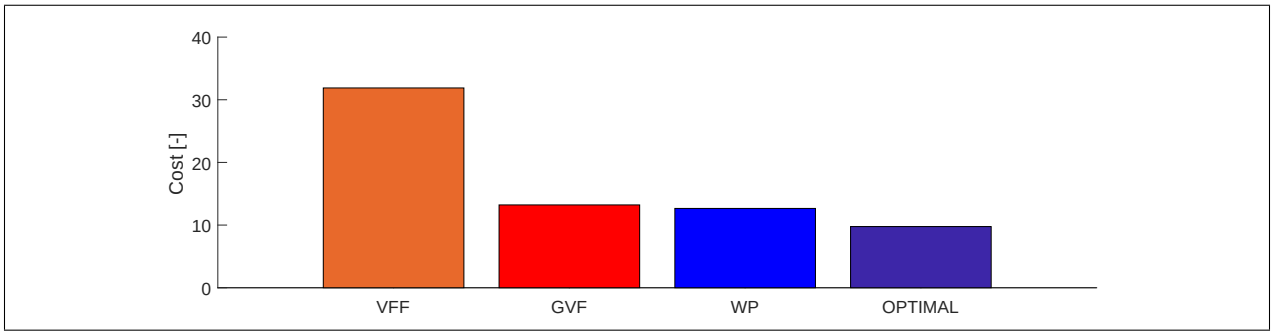


**Fig. 7 Cost performance for various UAV guidance methods**

## VI. Conclusion

A gradient vector field for path following and circular obstacle avoidance was optimized and shown to have similar performance to waypoint avoidance without the need to re-plan the mission path. The obstacle avoidance GVF acts on

the same principle as VFF, however guidance vectors are given circulation which aid in returning the UAV back to the planned path without intervention. A summary of the simulation costs for the scenario presented is shown in Table 1.

**Table 1 Obstacle Avoidance Method's Performance Summary**

| Method | Cost [-] | Returns to path quickly | Avoids obstacle without replanning |
|---|---|---|---|
| VFF | 31.8 | | ✓ |
| GVF | 13.2 | ✓ | ✓ |
| WP | 12.7 | ✓ | |

In literature, singularities in summed fields and scalar convergence and circulation terms were not optimized for avoidance. Singularities in summed GVFs were identified by numerically finding locations where vector field magnitudes were null in a summed field. It was shown adding circulation to a repulsive GVF remove singularities from a UAVs path and reduce path deviation cost function by 72%. Decay radius and circulation values were determined by minimizing a path deviation cost function. The improved GVF guidance was shown to have a reduced path deviation cost in comparison to potential field and traditional waypoint guidance. Increasing the number of deviation waypoints may provide guidance with lower cost than GVF, however when re-planning a path is not possible, such as instances where a ground station is not reachable, GVF provides a low cost method that can be computed on-board a UAV for avoiding obstacles without the need to re-plan the path. Future work to improve vector field for avoidance may include optimizing field parameters at each time step, potentially increasing time spent on the sensor line.

## References


[1] Fernandez Galarreta, J., Kerle, N., and Gerke, M., "UAV-based urban structural damage assessment using object-based image analysis and semantic reasoning," *Natural Hazards and Earth System Science*, Vol. 15, No. 6, 2015, pp. 1087–1101. doi:10.5194/nhess-15-1087-2015, URL http://www.nat-hazards-earth-syst-sci.net/15/1087/2015/.

[2] Remondino, F., Barazzetti, L., Nex, F., Scaioni, M., and Sarazzi, D., "UAV PHOTOGRAMMETRY FOR MAPPING AND 3D MODELING – CURRENT STATUS AND FUTURE PERSPECTIVES," *ISPRS - International Archives of the Photogrammetry, Remote Sensing and Spatial Information Sciences*, Vol. XXXVIII-1/C22, 2012, pp. 25–31. doi: 10.5194/isprsarchives-XXXVIII-1-C22-25-2011, URL http://www.int-arch-photogramm-remote-sens-spatial-inf-sci.net/XXXVIII-1-C22/25/2011/.

[3] Frew, E. W., "Cooperative standoff tracking of uncertain moving targets using active robot networks," *Robotics and Automation, 2007 IEEE International Conference on*, IEEE, 2007, pp. 3277–3282. URL http://ieeexplore.ieee.org/abstract/document/4209596/.

[4] Oh, H., Kim, S., Shin, H.-S., Tsourdos, A., and White, B., "Coordinated standoff tracking of groups of moving targets using multiple UAVs," *Control & Automation (MED), 2013 21st Mediterranean Conference on*, IEEE, 2013, pp. 969–977. URL http://ieeexplore.ieee.org/abstract/document/6608839/.

[5] Hyondong Oh, Seungkeun Kim, Hyo-sang Shin, and Tsourdos, A., "Coordinated standoff tracking of moving target groups using multiple UAVs," *IEEE Transactions on Aerospace and Electronic Systems*, Vol. 51, No. 2, 2015, pp. 1501–1514. doi:10.1109/TAES.2015.140044, URL http://ieeexplore.ieee.org/document/7126199/.

[6] Oliveira, T., Aguiar, A. P., and Encarnacao, P., "Moving Path Following for Unmanned Aerial Vehicles With Applications to Single and Multiple Target Tracking Problems," *IEEE Transactions on Robotics*, Vol. 32, No. 5, 2016, pp. 1062–1078. doi:10.1109/TRO.2016.2593044, URL http://ieeexplore.ieee.org/document/7553466/.

[7] Borenstein, J., and Koren, Y., "Real-time obstacle avoidance for fast mobile robots in cluttered environments," *Robotics and Automation, 1990. Proceedings., 1990 IEEE International Conference on*, IEEE, 1990, pp. 572–577. URL http://ieeexplore.ieee.org/abstract/document/126042/.

[8] Borenstein, J., and Koren, Y., "The vector field histogram-fast obstacle avoidance for mobile robots," *IEEE transactions on robotics and automation*, Vol. 7, No. 3, 1991, pp. 278–288. URL http://ieeexplore.ieee.org/abstract/document/88137/.

[9] Griffiths, S., "Vector Field Approach for Curved Path Following for Miniature Aerial Vehicles," American Institute of Aeronautics and Astronautics, 2006. doi:10.2514/6.2006-6467, URL http://arc.aiaa.org/doi/10.2514/6.2006-6467.

[10] Goncalves, V. M., Pimenta, L. C. A., Maia, C. A., and Pereira, G. A. S., "Artificial vector fields for robot convergence and circulation of time-varying curves in n-dimensional spaces," IEEE, 2009, pp. 2012–2017. doi:10.1109/ACC.2009.5160350, URL http://ieeexplore.ieee.org/document/5160350/.

[11] Gonçalves, V. M., Pimenta, L. C., Maia, C. A., Pereira, G. A., Dutra, B. C., Michael, N., Fink, J., and Kumar, V., "Circulation of curves using vector fields: actual robot experiments in 2D and 3D workspaces," *Robotics and Automation (ICRA), 2010 IEEE International Conference on*, IEEE, 2010, pp. 1136–1141.

[12] Gonçalves, V. M., Pimenta, L. C., Maia, C. A., Dutra, B. C., and Pereira, G. A., "Vector fields for robot navigation along time-varying curves in $ n $-dimensions," *IEEE Transactions on Robotics*, Vol. 26, No. 4, 2010, pp. 647–659. URL http://ieeexplore.ieee.org/abstract/document/5504176/.

[13] Technology, C. C., "," , 2018. URL http://www.cloudcaptech.com/.

[14] Martin, L., "Kestral Flight Systems And Autopilot," , 2018. URL https://www.lockheedmartin.com/en-us/products/procerus-technologies/kestrel.html.

[15] DroneCode, "Pixhawk 1 Flight Controller Guide," , 2018. URL https://docs.px4.io/en/flight_controller/pixhawk.html.

[16] Khatib, O., "Real-time obstacle avoidance for manipulators and mobile robots," *The international journal of robotics research*, Vol. 5, No. 1, 1986, pp. 90–98. URL http://journals.sagepub.com/doi/abs/10.1177/027836498600500106.

[17] Rimon, E., "Exact Robot Navigation Using Artificial Potential Functions.pdf," , 1992.

[18] Koren, Y., and Borenstein, J., "Potential Field Methods and their inherent limitions for morbile robot navigation.pdf," , 1991. URL http://ieeexplore.ieee.org/document/131810/.

[19] Liu, Y., and Zhao, Y., "A virtual-waypoint based artificial potential field method for UAV path planning," *Guidance, Navigation and Control Conference (CGNCC), 2016 IEEE Chinese*, IEEE, 2016, pp. 949–953. URL http://ieeexplore.ieee.org/abstract/document/7828913/.

[20] Kim, D. H., "Escaping route method for a trap situation in local path planning," *International Journal of Control, Automation and Systems*, Vol. 7, No. 3, 2009, pp. 495–500. doi:10.1007/s12555-009-0320-7, URL http://link.springer.com/10.1007/s12555-009-0320-7.

[21] Goerzen, C., Kong, Z., and Mettler, B., "A Survey of Motion Planning Algorithms from the Perspective of Autonomous UAV Guidance," *Journal of Intelligent and Robotic Systems*, Vol. 57, No. 1-4, 2010, pp. 65–100. doi:10.1007/s10846-009-9383-1, URL http://link.springer.com/10.1007/s10846-009-9383-1.

[22] Lei Tang, Songyi Dian, Gangxu Gu, Kunli Zhou, Suihe Wang, and Xinghuan Feng, "A novel potential field method for obstacle avoidance and path planning of mobile robot," IEEE, 2010, pp. 633–637. doi:10.1109/ICCSIT.2010.5565069, URL http://ieeexplore.ieee.org/document/5565069/.

[23] Li, G., Yamashita, A., Asama, H., and Tamura, Y., "An efficient improved artificial potential field based regression search method for robot path planning," IEEE, 2012, pp. 1227–1232. doi:10.1109/ICMA.2012.6283526, URL http://ieeexplore.ieee.org/document/6283526/.

[24] Sujit, P., Saripalli, S., and Sousa, J. B., "Unmanned Aerial Vehicle Path Following: A Survey and Analysis of Algorithms for Fixed-Wing Unmanned Aerial Vehicless," *IEEE Control Systems*, Vol. 34, No. 1, 2014, pp. 42–59. doi:10.1109/MCS.2013.2287568, URL http://ieeexplore.ieee.org/document/6712082/.

[25] Nelson, D. R., "Cooperative control of miniature air vehicles," 2005. URL http://scholarsarchive.byu.edu/etd/1095/.

[26] Nelson, D. R., Barber, D. B., McLain, T. W., and Beard, R. W., "Vector field path following for small unmanned air vehicles," *American Control Conference, 2006*, IEEE, 2006, pp. 7–pp. URL http://ieeexplore.ieee.org/abstract/document/1657648/.

[27] Nelson, D., Barber, D., McLain, T., and Beard, R., "Vector Field Path Following for Miniature Air Vehicles," *IEEE Transactions on Robotics*, Vol. 23, No. 3, 2007, pp. 519–529. doi:10.1109/TRO.2007.898976, URL http://ieeexplore.ieee.org/document/4252175/.

[28] Miao, Z., Thakur, D., Erwin, R. S., Pierre, J., Wang, Y., and Fierro, R., "Orthogonal vector field-based control for a multi-robot system circumnavigating a moving target in 3D," *Decision and Control (CDC), 2016 IEEE 55th Conference on*, IEEE, 2016, pp. 6004–6009. URL http://ieeexplore.ieee.org/abstract/document/7799191/.

[29] Gerlach, A. R., *Autonomous Path-Following by Approximate Inverse Dynamics and Vector Field Prediction*, University of Cincinnati, 2014. URL http://search.proquest.com/openview/432d738d856bf0a9b46acea1b1eee08f/1?pq-origsite=gscholar&cbl=18750&diss=y.

[30] Jung, W., Lim, S., Lee, D., and Bang, H., "Unmanned Aircraft Vector Field Path Following with Arrival Angle Control," *Journal of Intelligent & Robotic Systems*, Vol. 84, No. 1-4, 2016, pp. 311–325. doi:10.1007/s10846-016-0332-5, URL http://link.springer.com/10.1007/s10846-016-0332-5.

[31] Panagou, D., "Motion planning and collision avoidance using navigation vector fields," *Robotics and Automation (ICRA), 2014 IEEE International Conference on*, IEEE, 2014, pp. 2513–2518. URL http://ieeexplore.ieee.org/abstract/document/6907210/.